1 **Magnetospheric chaos and dynamical complexity response during storm time disturbance**

2 Irewola Aaron Oludehinwa[1], Olasunkanmi Isaac Olusola[1], Olawale Segun Bolaji[1,2], Olumide
3 Olayinka Odeyemi[1], Abdullahi Ndzi Njah[1]

4 [1]Department of Physics, University of Lagos, Nigeria

5 [2]Department of Physics, University of Tasmania, Australia

6 **Abstract**

7 In this study, we examine the magnetospheric chaos and dynamical complexity response to the

8 disturbance storm time (D_{st}) and solar wind electric field (VB_s) during different categories of

9 geomagnetic storm (minor, moderate and major geomagnetic storm). The time series data of the

10 D_{st} and VB_s are analyzed for the period of nine years using nonlinear dynamics tools (Maximal

11 Lyapunov Exponent, MLE, Approximate Entropy, ApEn and Delay Vector Variance, DVV). We

12 found a significant trend between each nonlinear parameter and the categories of geomagnetic

13 storm. The MLE and ApEn values of the D_{st} indicate that chaotic and dynamical complexity

14 responses are high during minor geomagnetic storms, reduce at moderate geomagnetic storms and

15 decline further during major geomagnetic storms. However, the MLE and ApEn values obtained

16 from VB_s indicate that chaotic and dynamical complexity response are high with no significant

17 difference between the periods that are associated with minor, moderate and major geomagnetic

18 storms. The test for nonlinearity in the D_{st} time series during major geomagnetic storm reveals the

19 strongest nonlinearity features. Based on these findings, the dynamical features obtained in the

20 VB_s as input and D_{st} as output of the magnetospheric system suggest that the magnetospheric

21 dynamics is nonlinear and the solar wind dynamics is consistently stochastic in nature.

22 ***Keywords***: D_{st} signals, Solar wind electric field (VB_s) signals, Geomagnetic storm, Chaotic

23 behaviour, Dynamical complexity, Nonlinearity.

1.0 Introduction

The response of chaos and dynamical complexity behaviour with respect to magnetospheric dynamics varies. This is due to changes in the interplanetary electric fields imposed on the magnetopause and those penetrating the inner magnetosphere and sustaining convection thereby initiating geomagnetic storm (Pavlos et al. 1992). A prolonged southward turning of interplanetary magnetic field (IMF,B_z), which indicates that solar wind-magnetosphere coupling is in-progress was confirmed on many occasions for which such geomagnetic storm was driven by Corotating Interaction Regions (CIRs), or by the sheath preceding an interplanetary coronal mass ejection (ICME) or by a combination of the sheath and an ICME magnetic cloud (Russell et al. 1974; Burton et al.1975; Gonzalez and Tsurutani, 1987; Tsurutani et al. 1988; Cowley, 1995; Tsutomu, 2002; Yurchyshyn et al. 2004; Kozyra et al. 2006; Echer et al. 2008; Meng et al. 2019; Tsurutani et al. 2020). Notably, the introduction of Disturbance Storm Time (D_{st}) index (Sugiura, 1964; Sugiura and Kamei, 1991) unveil the quantitative measure of the total energy of the ring current particles. Therefore, the D_{st} index remains one of the most popular global indicators that can precisely reveal the severity of a geomagnetic storm (Dessler and Parker, 1959).

The D_{st} fluctuations exhibit different signatures for different categories of geomagnetic storm. Ordinarily, one can easily anticipate that fluctuations in a D_{st} signal appear chaotic and complex. These may arise from the changes in the interplanetary electric fields driven by the solar wind-magnetospheric coupling processes. At different categories of geomagnetic storm, fluctuations in the D_{st} signals differ (Oludehinwa et al. 2018). One obvious reason is that as the intensity of the geomagnetic storm increases, the fluctuation behaviour in the D_{st} signal becomes more complex and nonlinear in nature. It has been established that the electrodynamic response of the magnetosphere to solar wind driver are non-autonomous in nature (Price and Prichard, 1993; Price

48   et al. 1994; Johnson and Wings, 2005). Therefore, the chaotic analysis of the magnetospheric time

49   series must be related to the concept of input-output dynamical process. Consequently, it is

50   necessary to examine the chaotic behaviour of the solar wind electric field (VB_s) as input signals

51   and the magnetospheric activity index (D_{st}) as output during different categories of geomagnetic

52   storms.

53   Several works have been presented on the chaotic and dynamical complexity behaviour of the

54   magnetospheric dynamics based on autonomous concept, i.e using the time series data of

55   magnetospheric activity alone such as auroral electrojet (AE), Amplitude Lower (AL) and D_{st}

56   index (Vassiliadis et al.1990; Baker and Klimas, 1990; Vassiliadis et al.1991; Shan et al. 1991;

57   Pavlos et al. 1994; Klimas et al. 1996; Valdivia et al. 2005; Mendes et al. 2017; Consolini, 2018).

58   They found evidence of low-dimensional chaos in the magnetospheric dynamics. For instance, the

59   report by Vassiliadis et al. (1991) shows that the computation of Lyapunov exponent for AL index

60   time series gives a positive value of Lyapunov exponent indicating the presence of chaos in the

61   magnetospheric dynamics. Unnikrishnan, (2008) studied the deterministic chaotic behaviour in the

62   magnetospheric dynamics under various physical conditions using AE index time series and found

63   that the seasonal mean value of Lyapunov exponent in winter season during quiet periods ($0.7 \pm$

64     $0.11\ min^{-1}$) is higher than that of the stormy periods ($0.36 \pm 0.09\ min^{-1}$). Balasis et al. (2006)

65   examined the magnetospheric dynamics in the D_{st} index time series from pre-magnetic storm to

66   magnetic storm period using fractal dynamics. They found that the transition from anti-persistent

67   to persistent behaviour indicates that the occurrence of an intense geomagnetic storm is imminent.

68   Balasis et al. (2009) further reveal the dynamical complexity behaviour in the magnetospheric

69   dynamics using various entropy measures. They reported a significant decrease in dynamical

70   complexity and an accession of persistency in the D_{st} time series as the magnetic storm

71   approaches. Recently, Oludehinwa et al. (2018) examined the nonlinearity effects in D_{st} signals

72   during minor, moderate and major geomagnetic storm using recurrence plot and recurrence

73   quantification analysis. They found that the dynamics of the D_{st} signal is stochastic during minor

74   geomagnetic storm periods and deterministic as the geomagnetic storm increases.

75   Also, studies describing the solar wind and magnetosphere as non-autonomous system have been

76   extensively investigated. Price et al. (1994) examine the nonlinear input-output analysis of AL

77   index and different combinations of interplanetary magnetic field (IMF) with solar wind

78   parameters as input function. They found that only a few of the input combinations show any

79   evidence whatsoever for nonlinear coupling between the input and output for the interval

80   investigated. Pavlos et al. (1999) presented further evidence of magnetospheric chaos. They

81   compared the observational behaviour of the magnetospheric system with the results obtained by

82   analyzing different types of stochastic and deterministic input-output systems and asserted that a

83   low dimensional chaos is evident in magnetospheric dynamics. Devi et al. (2013) studied the

84   magnetospheric dynamics using AL index with the southward component of IMF, (Bz) and

85   observed that the magnetosphere and turbulent solar wind have values corresponding to nonlinear

86   dynamical system with chaotic behaviour. The modeling and forecasting approach have been

87   applied to magnetospheric time series using nonlinear models (Valdivia et al. 1996; Vassiliadis et

88   al. 1999; Vassiliadis, 2006; Balikhin et al. 2010). These efforts have improved our understanding

89   with regards to the facts that nonlinear dynamics can reveal some hidden dynamical information

90   in the observational time series. In addition to these nonlinear effects in D_{st} signals, a measure of

91   the exponential divergence and convergence within the trajectories of a phase space known as

92   Maximal Lyapunov Exponent (MLE), which has the potential to depict the chaotic behavior in the

93   D_{st} and VB_s time series during a minor, moderate and major geomagnetic storm have not been

94 investigated. In addition, to the best of our knowledge, computation of Approximate Entropy

95 (ApEn) that depicts the dynamical complexity behaviour during different categories of

96 geomagnetic storm has not been reported in the literature. The test for nonlinearity through delay

97 vector variance (DVV) analysis that establishes the degree at which nonlinearity response in D_{st}

98 time series during minor, moderate and major geomagnetic storms is not well known. It is worth

99 to note that understanding the dynamical characteristics in the D_{st} and VB_s signals at different

100 categories of geomagnetic storms will provide useful diagnostic information to different conditions

101 of space weather phenomenon. Consequently, this study attempts to carry out comprehensive

102 numerical analysis to unfold the chaotic and dynamical complexity behaviour in the D_{st} and VB_s

103 signals during minor, moderate and major geomagnetic storm. In section 2, our methods of data

104 acquisition are described. Also, the nonlinear analysis that we employed in this investigation are

105 detailed. In section 3, we unveiled our results and engage the discussion of results in section 5.

106 **2.0 Description of the Data and Nonlinear Dynamics**

107 The D_{st} index is derived by measurements from ground-based magnetic stations at low-latitudes

108 observatories around the world and depicts mainly the variation of the ring current, as well as the

109 Chapman-Ferraro Magnetopause currents, and tail currents to a lesser extent (Sugiura, 1964; Love

110 and Gannon, 2009). Due to its global nature, D_{st} time series provides a measure of how intense a

111 geomagnetic storm was (Dessel and Parker, 1959). In this study, we considered D_{st} data for the

112 period of nine years from January to December between 2008 and 2016 which were downloaded

113 from the World Data Centre for Geomagnetism, Kyoto, Japan (http://wdc.kugi-kyoto-

114 u.ac.jp/Dstae/index.html). The sampling time of D_{st} and VB_s time series data was 1-hour. We use

115 the classification of geomagnetic storms as proposed by Gonzalez et al. (1994) such that D_{st} index

116 value in the ranges $0 \leq Dst \leq -50nT$, $-50nT \leq Dst \leq -100nT$, $-100nT \leq Dst \leq -250nT$

117   are classified as minor, moderate and major geomagnetic storms respectively and each month is

118   being classified based on its minimum Dst value. The solar wind electric field (VB_s) data are

119   archived from the National Aeronautics and Space Administration, Space Physics Facility

120   (http://omniweb.gsfc.nasa.gov). It is well known that the dynamics of the solar wind contribute to

121   the driving of the magnetosphere (Burton et al. 1975). Furthermore, we took the solar wind electric

122   field (VB_s) as the input signal (Price and Prichard, 1993; Price et al. 1994). The VB_s was

123   categorized according to the periods of minor, moderate and major geomagnetic storm. Then, the

124   D_{st} and VB_s time series were subjected to a variety of nonlinear analytical tools explained as

125   follow:

126   **2.1 Phase Space Reconstruction and Observational time series**

127   An observational time series can be defined as a sequence of scalar measurements of some

128   quantity, which is a function of the current state of the system taken at multiples of a fixed sampling

129   time. In nonlinear dynamics, the first step in analyzing an observational time series data is to

130   reconstruct an appropriate state space of the system. Takens, (1981) and Mane, (1981) stated that

131   one time series or a few simultaneous time series are converted to a sequence of vectors. This

132   reconstructed phase space has all the dynamical characteristic of the real phase space provided the

133   time delay and embedding dimension are properly specified.

134    $$X(t) = [x(t), x(t + \tau), x(t + 2\tau), \ldots, x(t + (m-1)\tau]^T \qquad (1)$$

135   where $X(t)$ is the reconstructed phase space, $x(t)$ is the original time series data, τ is the time

136   delay and m is the embedding dimension. An appropriate choice of τ and m are needed for the

137   reconstruction phase space which is determined by average mutual information and false nearest

138   neighbour respectively.

2.2 Average Mutual Information (AMI)

The method of Average Mutual Information (AMI) is one of the nonlinear techniques used to determine the optimal time delay (τ) required for phase space reconstruction in observational time series. The time delay mutual information was proposed by Fraser and Swinney, (1986) instead of autocorrelation function. This method takes into account nonlinear correlations within the time series data. It measures how much information can be predicted about one time series point, given full information about the other. For instance, the mutual information between x_i and $x_{(i+\tau)}$ quantifies the information in state $x_{(i+\tau)}$ under the assumption that information at the state x_i is known. The AMI for a time series, $x(t_i), \quad i = 1,2,\dots,N$ is calculated as:

$$I(T) = \sum_{x(t_i),\ x(t_i+T)} P(x(t_i), x(t_i + T)) \times \log_2 \left[\frac{P(x(t_i),x(t_i+T))}{P(x(t_i))\, P(x(t_i+T))} \right] \qquad (2)$$

Where $x(t_i)$ is the ith element of the time series, $T = k\Delta t \ \ (k = 1,2,\dots,k_{max})$, $P(x(t_i))$ is the probability density at $x(t_i)$, $P(x(t_i), x(t_i + T))$ is the joint probability density at the pair $x(t_i), x(t_i + T)$. The time delay (τ) of the first minimum of AMI is chosen as optimal time delay (Fraser and Swinney, 1986). Therefore, the AMI was applied to the D_{st} and VB_s time series and the plot of AMI against time delay is shown in Figure (3). We notice that the AMI showed the first local minimum at roughly ($\tau = 15hr$). Furthermore, the values of τ near this value of (~15hr) maintain constancy for both VBs and D_{st}. In the analysis ($\tau = 15hr$) was used as the optimal time delay for the computation of maximal Lyapunov exponent.

2.3 False Nearest Neighbour (FNN)

In determining the optimal choice of embedding dimension (m), the false nearest neighbour method was used in the study. It was suggested by Kennel et al. (1992). The concept is based on how the number of neighbours of a point along a signal trajectory changes with increasing embedding dimension. With increasing embedding dimension, the false neighbour will no longer be neighbours, therefore by examining how the number of neighbours changes as a function of dimension, an appropriate embedding dimension can be determined. For instance, suppose we have a one-dimensional time series. We can construct a time series $y(t)$ of D-dimensional points from the original one-dimensional time series $x(t)$ as follows:

$$y(t) = (x(t), x(t+\tau), \dots, x(t+(D-1)\tau) \qquad (3)$$

where D is embedding dimension. Using the formular from Kennel et al. (1992); Wallot and Monster, (2018). If we have a D-dimensional phase space and denote the rth nearest neighbour of a coordinate vector $y(t)$ by $y^{(r)}(t)$, then the square of the Euclidean distance between $y(t)$ and the rth nearest neighbor is:

$$R_D^2(t,r) = \sum_{k=0}^{D-1} \left[x(t+k\tau) - x^{(r)}(t+k\tau) \right]^2 \qquad (4)$$

Now applying the logic outlined above, we can go from a D-dimensional phase space to $(D+1)$ dimensional phase space by time-delay embedding, adding a new coordinate to $y(t)$, and ask what is the squared distance between $y(t)$ and the same rth nearest neighbour:

$$R_{D+1}^2(t,r) = R_D^2(t,r) + \left[x(t+D\tau) - x^{(r)}(t+D\tau) \right]^2 \qquad (5)$$

As explained above, if the one-dimensional time series is already properly embedded in D dimensions, then the distance R between $y(t)$ and the rth nearest neighbour should not

181   appreciably change by some distance criterion $R_{tol}(i.e\ R < R_{tol})$. Moreover, the distance of the

182   nearest neighbour when embedded into the next higher dimension relative to the size of the

183   attractor should be less than some criterion $A_{tol}(i.e\ R_{D+1} < A_{tol})$. Doing this for the nearest

184   neighbour of each coordinate will result on many false nearest neighbours when embedding is

185   insufficient or in few (or no) false neighbours when embedding is sufficient. In the analysis, the

186   FNN was applied to the D_{st} and VB_s time series to detect the optimal value of embedding

187   dimension(m). Figure (4) shows a sample plot of the percentage of false nearest neighbour against

188   embedding dimension in one of the months under investigation (other months show similar results,

189   thus for brevity we depict only one of the results). We notice that the false nearest neighbor attains

190   its minimum value at $m \geq 5$ indicating that embedding dimension (m) from $m \geq 5$ are optimal

191   values. Therefore, $m = 5$ was used for the computation of maximal Lyapunov exponent.

192   **2.4 Maximal Lyapunov Exponent (MLE)**

193   The Maximal Lyapunov Exponent (MLE) is one of the most popular nonlinear dynamics tool used

194   for detecting chaotic behaviour in a time series data. It describes how small changes in the state of

195   a system grow at an exponential rate and eventually dominate the behaviour. An important

196   indication of chaotic behavior of a dissipative deterministic system is the existence of a positive

197   Lyapunov Exponent. A positive MLE signifies divergence of trajectories in one direction or

198   expansion of an initial volume in this direction. On the other hand, a negative MLE exponent

199   implies convergence of trajectories or contraction of volume along another direction. The

200   algorithm proposed by Wolf et al. (1985) for estimating MLE is employed to compute the chaotic

201   behavior of the D_{st} and VB_s time series at minor, moderate and major geomagnetic storm. Other

202   methods of determining MLE includes Rosenstein's method, Kantz's method and so on. In this

203   study, the MLE at minor, moderate and major geomagnetic storms periods was computed with

204     $m = 5$ and $\tau = 15hr$ as shown in figures 5 & 6 (bar plots) for D_{st} and VB_s. The calculation of

205   MLE is explained as follows: given a sequence of vector $x(t)$, an m-dimensional phase space is

206   formed from the observational time series through embedding theorem as

207
$$\{x(t), x(t + \tau), \dots, x(t + (m - 1)\tau)\} \tag{6}$$

208   Where m and τ are as defined earlier, after reconstructing the observational time series, the

209   algorithm locates the nearest neighbour (in Euclidean sense) to the initial point $\{x(t_0), \dots, x(t_0 +$

210     $(m - 1)\tau\}$ and denote the distance between these two points $L(t_0)$. At a later point t_1, the initial

211   length will have evolved to length $L'(t_1)$. Then the MLE is calculated as:

212
$$\lambda = \frac{1}{t_M - t_0} \sum_{k=1}^{M} \log_2 \frac{L'(t_k)}{L(t_{k-1})} \tag{7}$$

213   M is the total number of replacement steps. We look for a new data point that satisfies two criteria

214   reasonably well: its separation, $L(t_1)$, from the evolved fiducial point is small. If an adequate

215   replacement point cannot be found, we retain the points that were being used. This procedure is

216   repeated until the fiducial trajectory has traversed the entire data

217   **2.5 Approximate Entropy (ApEn)**

218   Approximate Entropy (ApEn) measures the dynamical complexity in observational time series. It

219   was proposed by Pincus, (1991), it provides a generalized measure of regularity, such that it

220   accounts for the logarithm likehood in the observational time series. For instance, a dataset of

221   length, N, that repeat itself for m points within a boundary will again repeat itself for $m + 1$ points.

222   Because of its computational advantage, ApEn has been widely used in many areas of disciplines

223   to study dynamical complexity (Pincus and Kalman (2004); Pincus and Goldberger (1994);

224   McKinley et al. (2011); Kannathan et al. (2005); Balasis et al. (2009); Shujuan and Weidong,

225   (2010); Moore and Marchant (2017)). The ApEn is computed using the formula below:

226   $$ApEn(m, r, N) = \frac{1}{N-m+1} \sum_{i=1}^{N-m+1} \log C_i^m(r) - \frac{1}{N-m} \sum_{i=1}^{N-m} \log C_i^m(r) \qquad (8)$$

227   where $C_i^m(r) = \frac{1}{N-m+1} \sum_{j=1}^{N-m+1} \Theta\left(r - \|x_i - x_j\|\right)$ is the correlation integral and r is the tolerance.

228   To compute the ApEn for the D_{st} and VB_s time series classified at minor, moderate and major

229   geomagnetic storm from 2008 to 2016, we choose $(m = 3, \tau = 1hr)$. We refer the works of

230   Pincus, (1991); Kannathal et al. (2005); and Balasis et al. (2009) to interested readers where all

231   the computational steps regarding ApEn were explained in details. Figures (5 & 6) depict the stem

232   plots of ApEn for D_{st} and (VB_s) from 2008 to 2016.

233   **2.6 Delay Vector Variance (DVV) analysis**

234   The Delay Vector Variance (DVV) is a unified approach in analyzing and testing for nonlinearity

235   in a time series (Gautama et al. 2004; Mandic et al. 2007). The basic idea of the DVV is that, if

236   two delay vectors of a predictable signal are close to each other in terms of the Euclidean distance,

237   they should have similar target. For instance, when a time delay (τ) is embedded into a time series

238   $x(k), \ k = 1, 2, \dots, N$, then a reconstructed phase space vector is formed which represents a set of

239   delay vectors (DVs) of a given dimension.

240   $$X(k) = [X_{k-m\tau}, \dots, X_{k-\tau}]^T \qquad (9)$$

241   Reconstructing the phase space, a set (λ_k) is generated by grouping those DVs that are with a

242   certain Euclidean distance to DVs $(X(k))$. For a given embedding dimension (m), a measure of

243   unpredictability $\sigma *^2$ is computed over all pairwise Euclidean distance between delay vector as

244   $$d(i, j) = \|x(i) - x(j)\| \quad (i \neq j) \qquad (10)$$

245 Then, sets $\lambda_k(r_d)$ are generated as the sets which consist of all delay vectors that lie closer to $x(k)$

246 than a certain distance r_d.

247
$$\lambda_k(r_d) = \{x(i)\|x(k) - x(i)\| \leq r_d\} \tag{11}$$

248 For every set $\lambda_k(r_d)$, the variance of the corresponding target $\sigma *^2 (r_d)$ is

249
$$\sigma *^2 (r_d) = \frac{\frac{1}{N}\sum_{k=1}^{N} \sigma_k^2(r_d)}{\sigma_k} \tag{12}$$

250 where $\sigma *^2 (r_d)$ is target variance against the standardized distance indicating that Euclidean

251 distance will be varied in a manner standardized with respect to the distribution of pairwise

252 distance between DVs. Iterative Amplitude Adjusted Fourier Transform (IAAFT) method is used

253 to generate the surrogate time series (Kugiumtzis, 1999). If the surrogate time series yields DV

254 plots similar to the original time series and the scattered plot coincides with the bisector line, then

255 the original time series can be regarded as linear (Theiler et al. 1992; Gautama et al.2004; Imitaz,

256 2010; Jaksic et al. 2016). On the other hand, if the surrogate time series yield DV plot that is not

257 similar to that of the original time series, then the deviation from the bisector lines indicates

258 nonlinearity. The deviation from the bisector lines grows as a result of the degree of nonlinearity

259 in the observational time series.

260
$$t^{DVV} = \sqrt{\langle(\sigma^{*2}(r_d) - \frac{\sum_{i=1}^{N} \sigma_{s,i}^{*2}}{N_s})\rangle} \tag{13}$$

261 where $\sigma_{s,i}^{*2}(r_d)$ is the target variance at the span r_d for the ith surrogate. To carry out the test for

262 nonlinearity in the D_{st} signals, $m = 3$ and $n_d = 3$, the number of references DVs=200, and

263 number of surrogates, $N_s = 25$ was used in all the analysis. Then we examined the nonlinearity

264 response at minor, moderate and major geomagnetic storm.

3.0 Results

In this study, D_{st} and VB_s time series from January to December was analyzed for the period of nine years (2008 to 2016) to examine the chaotic and dynamical complexity response in the magnetospheric dynamics during the month of minor, moderate and major geomagnetic storms activity. Figures (1) & (2), display the samples of fluctuation signatures of D_{st} and VB_s signals classified as (a): the month of minor, (b): the month of moderate and (c): the month of major geomagnetic storm activity. The plot of Average Mutual information against time delay (τ) shown in Figure (3) depicts that the first local minimum of the AMI function was found to be roughly at $\tau = 15$hr. Furthermore, we notice that the values of τ near this value of (~15hr) maintain constancy for both VB_s and D_{st}. Also, in Figure (4), we display the plot of the percentage of false nearest neighbour against embedding dimension (m). It is obvious that a decrease in false nearest neighbour when increasing the embedding dimension drop steeply to zero at the optimal dimension($m = 5$), thereafter the false neighbours stabilizes at $m = 5$ for VB_s and D_{st}. Therefore, $m = 5$ and $\tau = 15$hr was used for the computation of MLE at different categories of geomagnetic storm, while $m = 3$ and $\tau = 1$hr are applied for the computation of ApEn values.

The results of MLE (bar plot) and ApEn (stem plot) for D_{st} at the month of minor, moderate and major geomagnetic storms activity are shown in Figure 5. During the month of minor geomagnetic storms activity, we notice that the value of MLE ranges between 0.07 and 0.14 for most of the months classified as minor geomagnetic storm. Similarly, the ApEn (stem plot) ranges between 0.59 and 0.83. It is obvious that strong chaotic behaviour with high dynamical complexity are associated with minor geomagnetic storms. During the month of moderate geomagnetic storm activity, (see b part of Figure (5)), we observe a reduction in MLE values (0.04~0.07) compared to minor geomagnetic storm periods. Within the observed values of MLE during the month of

288   moderate geomagnetic storms activity, we found a slight rise of MLE in the following months

289   (Mar 2008), (Apr 2011), (Jan 2012, Feb 2012, Apr 2012), (Jul 2015, Aug 2015, Sept 2015,

290   Oct2015, Nov 2015) and (Nov 2016). Also, the ApEn revealed a reduction in values between 0.44

291   and 0.57 at the month of moderate geomagnetic storms activity. The lowest values of ApEn were

292   noticed in the following months: May 2010, Mar 2011, and Jan 2016. During major geomagnetic

293   storm as shown in Figure 5, the minimum and maximum value of MLE is respectively 0.03 and

294   0.04 implying a very strong reduction of chaotic behaviour compared with the month of minor and

295   moderate geomagnetic storm activity. The lowest values of MLE were found in the months of Jul

296   2012, Jun 2013 and Mar 2015. Interestingly, further reduction in ApEn value (0.29~0.40) was as

297   well noticed during this period. Thus, during the month of major geomagnetic storm activity,

298   chaotic behaviour and dynamical complexity subsides significantly.

299   We display in Figure 6, the results of MLE and ApEn computation for the VB_s which has been

300   categorized according to the month of minor, moderate and major geomagnetic storm activity. The

301   values of MLE (bar plot) were between 0.06 and 0.20 for VB_s. The result obtained indicate strong

302   chaotic behaviour with no significant difference in chaoticity during minor, moderate and major

303   geomagnetic storm. Similarly, the results obtained from computation of ApEn (stem plot) for VB_s

304   depict a minimum value of 0.60 and peak value of 0.87 as shown in Figure 6. The ApEn values of

305   VB_s indicates high dynamical complexity response with no significant difference during the

306   periods of the three categories of geomagnetic storm investigated.

307   The test for nonlinearity in the D_{st} signals during the month of minor, moderate and major

308   geomagnetic storms activity was analyzed through the DVV analysis. Shown in Figure 9 is the

309   DVV plot and DVV scatter plot during minor geomagnetic storm for January 2009 and January

310   2014. We found that the DVV plots during the month of minor geomagnetic storms activity reveal

311   a slight separation between the original and surrogate data. Also, the DVV scatter plots shows a

312   slight deviation from the bisector line between the original and surrogate data which implies

313   nonlinearity. Also, during the month of moderate geomagnetic storm activity, we notice that the

314   DVV plot depicts a wide separation between the original and the surrogate data. Also, a large

315   deviation from the bisector line between the original and the surrogate data was also observed in

316   the DVV scatter plot as shown in Figure (8) thus indicating nonlinearity. In Figure (9), we display

317   samples of DVV plot and DVV scatter plot during major geomagnetic storm for Oct 2011 and Dec

318   2015. The original and the surrogate data showed a very large separation in the DVV plot during

319   the month of major geomagnetic storm activity. While the DVV scatter plot depict a very large

320   deviation from the bisector line between the original and the surrogate data which is also an

321   indication of nonlinearity. The DVV analysis of the VB_s time series during the month of minor,

322   moderate and major geomagnetic storm activity shown in Figures (10-12) revealed a slight

323   separation between the original and surrogate data with no significant difference between the

324   month of minor, moderate and major geomagnetic activity.

325   **4.0 Discussion of Results**

326   **4.1 The chaotic and dynamical complexity response in D_{st} during the months of minor,**

327   **moderate and major geomagnetic storms**

328   Our result shows that the values of MLE for D_{st} during the month of minor geomagnetic storm

329   activity are higher, indicating significant chaotic response during minor geomagnetic stormy

330   periods (see the bar plots in Figure 5). This increase in chaotic behaviour for D_{st} signals during

331   minor geomagnetic storm may be as a result of asymmetry features in the longitudinal distribution

332   of solar source region for the Corotating Interaction Regions (CIR) signatures responsible for the

333   development of geomagnetic storms (Turner et al. 2006; Kozyra et al. 2006). CIR generated

334   magnetic storms are generally weaker than ICME/MC generated storms (Richardson and Cane,

335   2011). Therefore, we suspect that the increase in chaotic behaviour during minor geomagnetic

336   storm is strongly associated with the asymmetry features in the longitudinal distribution of solar

337   source region for the Corotating Interaction Regions (CIR) signatures. For most of these periods

338   of moderate geomagnetic storms, the values of MLE decreases compared to the month of minor

339   geomagnetic storms activity. This revealed that as geomagnetic stormy events build up, the level

340   of unpredictability and sensitive dependence on initial condition (chaos) begin to decrease

341   (Lorentz, 1963; Stogaz, 1994). The chaotic behaviour during the month of major geomagnetic

342   storm decreases significantly compared with the month of moderate geomagnetic storm activity.

343   The reduction in chaotic response during the month of moderate and its further declines at major

344   geomagnetic storm activity may be attributed to the disturbance in the interplanetary medium

345   driven by sheath preceding an interplanetary coronal mass ejection (ICME) or combination of the

346   sheath and an ICME magnetic cloud (Echer et al. 2008; Tsurutani et al. 2003; Meng et al. 2019).

347   Notably, the dynamics of the solar wind-magnetospheric interaction are dissipative chaotic in

348   nature (Pavlos, 2012); and, the electrodynamics of the magnetosphere due to the flux of

349   interplanetary electric fields had a significant impact on the state of the chaotic signatures. For

350   instance, the observation of strong chaotic behaviour during the month of minor geomagnetic

351   storm activity suggests that the dynamics was characterized by a weak magnetospheric

352   disturbance. While the reduction in chaotic behaviour at moderate and major geomagnetic storm

353   period reveals the dynamical features with regards to when a strong magnetospheric disturbance

354   begins to emerge. Therefore, our observation of chaotic signatures at different categories of

355   geomagnetic storm has potential capacity to give useful diagnostic information about monitoring

356   space weather events. It is important to note that the features of D_{st} chaotic behaviour at different

357 categories of geomagnetic storm has not been reported in the literature to the best of our

358 knowledge. For example, previous study of Balasis et al. (2009, 2011) investigate dynamical

359 complexity behaviour using different entropy measures and revealed the existence of low

360 dynamical complexity in the magnetospheric dynamics and attributed it to ongoing large

361 magnetospheric disturbance (major geomagnetic storm). The work of Balasis et al. (2009, 2011)

362 where certain dynamical characteristic evolved in the D_{st} signal was limited to one year data

363 (2001). It is worthy to note that the year 2001, according to sunspot variations is a period of high

364 solar activity during solar cycle 23. It is characterized by numerous and strong solar eruptions that

365 were followed by significant magnetic storm activities. This confirms that on most of the days in

366 year 2001, the geomagnetic activity is strongly associated with major geomagnetic storm. The

367 confirmation of low dynamical complexity response in the D_{st} signal during major geomagnetic

368 storm agree with our current study. However, the idea of comparing the dynamical complexity

369 behaviour at different categories of geomagnetic storm and reveal its chaotic features was not

370 reported. This is the major reason why our present investigation is crucial to the understanding of

371 the level of chaos and dynamical complexity involved during different categories of geomagnetic

372 storm. As an extension to the single-year investigation done by Balasis et al. (2009, 2011) during

373 a major geomagnetic storm, we further investigated nine years data of D_{st} that covered minor,

374 moderate and major geomagnetic storm (see Figure (5), stem plots) and unveiled their dynamical

375 complexity behaviour. During major geomagnetic stormy periods, we found that the ApEn values

376 decrease significantly, indicating reduction in the dynamical complexity behaviour. This is in

377 agreement with the low dynamical complexity reported by Balasis et al. (2009, 2011) during a

378 major geomagnetic period. Finally, based on the method of DVV analysis, we found that test of

379   nonlinearity in the D_{st} time series during major geomagnetic storm reveals the strongest

380   nonlinearity features.

4.2 The chaotic and dynamical complexity behaviour in the VB_s as input signals.

382   The results of the MLE values for VB_s revealed a strong chaotic behaviour during the three

383   categories of geomagnetic storm. Comparing these MLE values during the month of minor to those

384   observed during moderate and major geomagnetic storm activity, the result obtained did not

385   indicate any significant difference in chaoticity (bar plots, Figure (6)). Also, the ApEn values of

386   VB_s during the periods associated with minor, moderate and major geomagnetic storm revealed

387   high dynamical complexity behaviour with no significant difference between the three categories

388   of geomagnetic storm investigated. These observations of high chaotic and dynamical complexity

389   behaviour in the dynamics of VB_s may be due to interplanetary discontinuities caused by the abrupt

390   changes in the interplanetary magnetic field direction and plasma parameters (Tsurutani et al.

391   2010). Also, the indication of high chaotic and dynamical complexity behaviour in VB_s signifies

392   that the solar wind electric field is stochastic in nature. The DVV analysis for VB_s revealed

393   nonlinearity features with no significant difference between the month of minor, moderate and

394   major geomagnetic storm activity. It is worth mentioning that the dynamical complexity behaviour

395   for VB_s is different from what was observed for D_{st} time series data. For instance, our results for

396   D_{st} times series revealed that the chaotic and dynamical complexity behaviour of the

397   magnetospheric dynamics are high during minor geomagnetic storm, reduce at moderate

398   geomagnetic storm and further decline during major geomagnetic storm. While the VB_s signal

399   revealed a high chaotic and dynamical complexity behaviour at all the categories of geomagnetic

400   storm period. Therefore, these dynamical features obtained in the VB_s as input signal and the D_{st}

401   as the output in describing the magnetosphere as a non-autonomous system further support the

402   finding of Donner et al. (2019) that found increase or no change in dynamical complexity

403   behaviour for VB_s and low dynamical complexity behaviour during storm using recurrence

404   method. Thus, suggesting that the magnetospheric dynamics is nonlinear and the solar wind

405   dynamics is consistently stochastic in nature.

406   **5.0 Conclusions**

407   This work has examined the magnetospheric chaos and dynamical complexity behaviour in the

408   disturbance storm time (D_{st}) and solar wind electric field (VB_s) as input during different categories

409   of geomagnetic storm. The chaotic and dynamical complexity behaviour during the month of

410   minor, moderate and major geomagnetic storm activity for solar wind electric field (VB_s) as input

411   and D_{st} as output of the magnetospheric system were analyzed for the period of 9 years using

412   nonlinear dynamics tools. Our analysis has shown a noticeable trend of these nonlinear parameters

413   (MLE and ApEn) and the categories of geomagnetic storm (minor, moderate and major). The MLE

414   and ApEn values of the D_{st} have indicated that the chaotic and dynamical complexity behaviour

415   are high during the month of minor geomagnetic storm, low during moderate geomagnetic storm

416   and further reduced during major geomagnetic storm activity. The values of MLE and ApEn

417   obtained from VB_s indicate that chaotic and dynamical complexity are high with no significant

418   difference during the periods of minor, moderate and major geomagnetic storm. Finally, the test

419   for nonlinearity in the D_{st} time series during major geomagnetic storm reveals the strongest

420   nonlinearity features. Based on these findings, the dynamical features obtained in the VB_s as input

421   and D_{st} as output of the magnetospheric system suggest that the magnetospheric dynamics is

422   nonlinear and the solar wind dynamics is consistently stochastic in nature.

423

424   **7.0 Acknowledgement**

425   The authors would like to acknowledge the World Data Centre for Geomagnetism, Kyoto, and the

426   National Aeronautics and Space Administration, Space Physics Facility (NASA) for making the

427   Dst data and solar wind plasma data available for research purpose.

428   **Declaration of Interest statement**

429   The authors declare that there is no conflict of interest.

430   **References**

431   Baker, D.N., Klimas, A.J., (1990). The evolution of weak to strong geomagnetic activity: An

432   interpretation in terms of deterministic chaos. J. GeoPhys. Res. Letts. Vol. 17, No. 1, PP. 41-

433   44.

434   Balasis, G., Daglis, I.A., Anastasiadia, A., Eftaxias, K., (2011). Detection of dynamical complexity

435   changes in Dst time series using entropy concepts and rescaled range analysis. W.Liu, M.

436   Fujimoto (eds.), The Dynamics Magnetosphere, IAGA Special Sopron Book Series 3, doi:

437   10.1007/978-94-007-0501-2_12, Springer Science+Business Media B.V. 2011.

438   Balasis, G., I.A. Daglis, C. Papadimitriou, M. Kalimeri, A. Anastasiadis, K. Eftaxias (2009).

439   Investigating dynamical complexity in the magnetosphere using various entropy measures,

440   J.Geophys.Res., 114, A0006, doi: 10.1029/2008JA 014035.

441   Balasis, G., I.A. Daglis, P. Kapiris, M.Mandea, D. Vassilliadis, K. Eftaxias (2006). From pre-storm

442   activity to magnetic storms: a transition described in terms of fractal dynamics, Ann.Geophys.,

443   24, 3557-3567, www.ann-geophys.net/24/3557/2006.

444 Balikhin, M.A., Boynton, R.J., Billings, S.A., Gedalin, M., Ganushkina, N., Coca, D., (2010). Data

445   based quest for solar wind-magnetosphere coupling function, Geophys.Res.Lett, 37, L24107,

446   doi: 10.1029/2010GL045733.

447 Burton, R.K., McPherron, R.L., Russell, C.T., (1975). An empirical relationship between

448   interplanetary conditions and Dst. Journal of Geophysical Research, Vol.80, No.31.

449 Consolini, G., (2018), Emergence of dynamical complexity in the Earth's magnetosphere, Machine

450   learning techniques for space weather, PP. 177-202, doi: 10.1016/B978-0-12-811788-0.00007-

451   X

452 Cowley, S.W.H., (1995). The earth's magnetosphere: A brief beginner's guide, EOS

453   Trans.Am.GeoPhys.Union, 76, 525.

454 Dessler, A.J., Parker, E.N., (1959). Hydromagnetic theory of magnetic storm. J. GeoPhys. Res, 64,

455   PP 2239-2259.

456 Devi, S.P., Singh, S.B., Sharma, A.S., (2013). Deterministic dynamics of the magnetosphere:

457   results of the 0-1 test. Nonlin. Processes Geophys., 20, 11-18, 2013, www.nonlin-processes-

458   geophys.net/20/11/2013, doi: 10. 5194/npg-20-11-2013.

459 Donner, R.V., Balasis, G., Stolbova,V., Georgiou, M., Weiderman, M., Kurths, J. (2019).

460   Recurrence-based quantification of dynamical complexity in the earth's magnetosphere at

461   geospace storm time scales. Journal of Geophysical Research: Space Physics, 124, 90-108,

462   doi: 10.1029/2018JA025318.

463 Echer, E., Gonzalez, D., Alves, M.V., (2006). On the geomagnetic effects of solar wind

464   interplanetary magnetic structures. Space Weather, Vol.4, S06001,

465   doi:10.1029/2005SW000200.

466 Echer, E., Gonzalez, W.D., Tsurutani, B.T., Gonzalez, A. L. C., (2008), Interplanetary conditions

467   causing intense geomagnetic storms ($D_{st} \leq -100nT$) during solar cycle 23 (1996–2006), J.

468   Geophys. Res., 113, A05221, doi:10.1029/2007JA012744.

469 Fraser, A.M., (1986). Using mutual information to estimate metric entropy, dimension and

470   entropies in chaotic system, Springer-Verlag, 1986, PP: 82-91.

471 Fraser, A.M., Swinney, H.L., (1986). Independent coordinates for strange attractors from mutual

472   information, Phys.Rev.A 33, 1134-1140.

473 Gautama, T., Mandic, D.P., Hulle, M.M.V., (2004). The delay vector variance method for detecting

474   determinism and nonlinearity in time series. Physica D, 190, 167-176, doi:

475   10.1016/j.physd.2003.11.001.

476 Gonzalez, W.D., Joselyn, J.A., Kamide, Y., Kroehl, H.W., Rostoker, G., Tsurutani, B.T.,

477   Vasyliunas, V.M., (1994). What is a geomagnetic storm? J. Geophys. Res.: Space Physics,

478   Vol. 99, issue A4, pg. 5771-5792, doi: 10.1029/93JA02867.

479 Gonzalez, W.D., Tsurutani, B.T., (1987). Criteria of interplanetary parameters causing intense

480   magnetic storm ($Dst < -100nT$). Planetary and Space Science,

481   https://ntrs.nasa.gov/search.jsp?R=198800068.

482 Horne, R.H., Glauert, S.A., Meredith, N.P., Boscher, D., Maget, V., Heynderickx, D., and Pitcford,

483 D. (2013). Space weather impacts on satellites and forecasting the Earths electron radiation

484 belts with SPACECAST. Space weather, **11,** 169 - 186

485 Imtiaz, A., (2010). Detection of nonlinearity and stochastic nature in time series by delay vector

486 variance method, International journal of Engineering & Technology, Vol. 10, No. 02.

487 Jaksic, V., Mandic, D.P., Ryan, K., Basu, B., Pakrashi V., (2016). A Comprehensive Study of the

488 Delay Vector Variance Method for Quantification of Nonlinearity in dynamical Systems.

489 *R.Soc.OpenSci.*, 2016: 3:150493, http://dx.doi.org/10.1098/rsos.150493.

490 Johnson, J.R., Wing, S., (2005), A solar cycle dependence of nonlinearity in magnetospheric

491 activity. J. Geophys. Res., 110, A04211, doi: 10.1029/2004JA010638.

492 Kannathal, N., M.L. Choo, U. R. Acharya, P. K. Sadasivan (2005). Entropies for detecting of

493 epilepsy in EEG, Computer Methods and Programs in Biomedicine (2005) 80, 187-194,

494 www.intl.elsevierhealth.com/journals/cmpb.

495 Kennel, M.B., R. Brown, H.D.I. Abarbanel (1992). Determining embedding dimension for phase-

496 space reconstruction using a geometrical construction, PHYSICAL REVIEW A, Volume 45,

497 Number 6.

498 Klimas, A.J., Vassilliasdis, D., Baker. D.N., Roberts, D.A., (1996). The organized nonlinear

499 dynamics of the magnetosphere. J. GeoPhys. Res. Vol.101, No. A6, PP 13089-13113.

500 Kozyra, J.U., Crowley, G., Emery, B.A., Fang, X., Maris, G., Mlynczak, M.G., Niciejewski, R.J.,

501 Palo, S.E., Paxton, L.J., Randall, C.E., Rong, P.P., Russell, J.M., Skinner, W., Solomon, S.C.,

502 Talaat, E.R., Wu, Q., Yee, J.H., (2006), Response of the Upper/Middle Atmosphere to Coronal

503   Holes and Powerful High-Speed Solar Wind Streams in 2003, Geophysical Monograph Series

504   167, 10.1029/167GM24.

505   Kugiumtzis, D., (1999). Test your surrogate before you test your nonlinearity, Phys. Rev. E, 60,

506   2808-2816.

507   Lorenz, E.N., (1963). Determining nonperiodic flow. J. Atmos.Sci.,20,130.

508   Love, J.J., Gannon, J.L. (2009). Revised Dst and the epicycles of magnetic disturbance: 1958-2007.

509   Ann.GeoPhys., 27, 3101-3131.

510   Mandic, D.P., Chen, M., Gautama, T., Van Hull, M.M., Constantinides, A., (2007). On the

511   Characterization of the Deterministic/Stochastic and Linear/Nonlinear Nature of Time Series.

512   *Proc.R.Soc*, 2008: A464, 1141-1160, doi: 10.1098/rspa. 2007.0154.

513   Mane, R., (1981). On the dimension of the compact invariant sets of certain nonlinear maps, D.Rand

514   and L.S.Young, eds, 1981.

515   Mckinley, R.A., Mclntire, L.K., Schmidt, R., Repperger, D.W., Caldwell, J.A., (2011). Evaluation

516   of Eye Metrics as a Detector of Fatigue. Human factor, 53 (4): 403-414, doi:

517   10.1177/0018720811411297.

518   Mendes, O., Dominques, M.O., Echer, E., Hajra, R., Menconi, V.E., (2017), Characterization of

519   high-intnesity, long-duration continuous auroral activitity (HILDCAA) events using

520   recurrence quantification analysis. Nonlin. Processes Geophys.,24,407-417, doi:10.5194/npg-

521   24-407-2017.

522   Meng, X., Tsurutani, B. T., Mannucci, A. J. (2019). The solar and interplanetary causes of

523   superstorms (minimum Dst ≤ -250 nT) during the space age. Journal of Geophysical Research:

524   Space Physics, 124, 3926–3948. https://doi.org/10.1029/2018JA026425.

525   Millan, H., Gharbarian-Alavijeh, B., Garcia-Fornaris, I., (2010). Nonlinear dynamics of mean daily

526   temperature and dewpoint time series at Babolsar, Iran, 1961-2005. Elsevier, Atmospheric

527   Research 98 (2010) 89-101, doi: 10.1016/j.atmosres.2010.06.001.

528   Moore, C., Marchant, T., (2017). The approximate entropy concept extended to three dimensions

529   for calibrated, single parameter structural complexity interrogation of volumetric images.

530   Physics in Medicine & Biology, 62(15).

531   Oludehinwa, I.A., Olusola, O.I., Bolaji, O.S., Odeyemi, O.O., (2018). Investigation of nonlinearity

532   effect during storm time disturbance, Adv. Space. Res, 62 (2018) 440-456, doi:

533   10.1016/j.asr.2018.04.032.

534   Omkar, P.T., Verma, P.L., (2013). Solar features and solar wind plasma parameters with

535   geomagnetic storms during the period of 2002-2006. Indian Journal of Applied Research,

536   Vol.3, Issue.5, ISSN-2249-555X.

537   Pavlos, G.P., (1994). The magnetospheric chaos: a new point of view of the magnetospheric

538   dynamics. Historical evolution of magnetospheric chaos hypothesis the past two decades.

539   Conference Proceeding of the 2nd Panhellenic Symposium held in Democritus University of

540   Thrace, Greece, 26-29, April, edited 1994.

541   Pavlos, G.P., (2012). Magnetospheric dynamics and Chaos theory

542 Pavlos, G.P., Athanasiu, M.A., Diamantidis, D., Rigas, A.G., Sarri, E.T., (1999). Comments and

543   new results about the magnetospheric chaos hypothesis. Nonlinear Processes in Geophysics

544   (1999) 6: 99-127.

545 Pavlos, G.P., Rigas, A.G., Dialetis, D., Sarris, E.T., Karakatsanis, L.P., Tsonis, A.A., (1992).

546   Evidence of chaotic dynamics in the outer solar plasma and the earth magnetosphere. Chaotic

547   dynamics: Theory and Practice, Edited by T. Bountis, Plenum Press, New York, Page. 327-

548   339, doi:10.1007/978-1-4615-3464-8_30.

549 Pincus, S.M., (1991). Approximate entropy as a measure of system complexity, Proc.Natl.Acad.Sci.

550   USA, Vol.88, PP. 2297-2301.

551 Pincus, S.M., Goldberger, A.L., (1994). Physiological time series analysis: what does regularity

552   quantify, The American Journal of Physiology, 266 (4): 1643-1656.

553 Pincus, S.M., Kalman, E.K., (2004). Irregularity, volatility, risk, and financial market time series,

554   Proceedings of the National Academy of Sciences, 101 (38): 13709-13714, doi:

555   10.1073/pnas.0405168101.

556 Price, C.P., Prichard, D., Bischoff, J.E., (1994). Nonlinear input/output analysis of the auroral

557   electrojet index. Journal of Geophysical Research, Vol.99, No: A7, PP: 227-238.

558 Price,C.P., Prichard, D., (1993). The Non-linear response of the magnetosphere: 30 October, 1978.

559   Geophysical Research Letters, Vol.20.

560 Richardson, I.G., Cane, H.V., (2011), Geoeffectiveness (D_{st} and K_p) of interplanetary coronal

561   mass ejections during 1995-2009 and implication for storm forecasting, Space Weather, 9,

562   S07005, doi:10.1029/2011SW000670.

563 Russell, C.T., (2001). Solar wind and Interplanetary Magnetic Field: A Tutorial. Space Weather,

564   Geophysical Monograph 125, Page: 73-89.

565 Russell, C.T., McPherron, R.L., Burton, R.K. (1974). On the cause of geomagnetic storms,

566   J.GeoPhys.Res., 79, 1105-1109.

567 Shujuan G., Weidong, Z., (2010). Nonlinear feature comparison of EEG using correlation

568   dimension and approximate entropy, 3rd international conference on biomedical engineering

569   and informatics.

570 Strogatz, S.H., (1994), Nonlinear dynamics and chaos with Application to physics, Biology,

571   chemistry and Engineering, New York, John Wiley & Sons.

572 Sugiura, M. (1964). Hourly Values of equatorial Dst for the IGY, Ann.Int. GeoPhys. Year, 35, 9-

573   45.

574 Takens, F., (1981). Detecting Strange Attractors in Turbulence in Dynamical Systems, D.*Rand &*

575   *L.Young Eds*, 1981: 898, 366-381.

576 Theiler, J., Eubank, S., Longtin, A., Galdrikian, B., Farmer, J.D., (1992), Testing for nonlinearity

577   in time series: The method of surrogate data, Physica D, 58, 77.

578 Tsurutani, B.T., Gonzalez, W. D., Tang, F., Akasofu, S.I., Smith, E.J., (1988), Origin of

579   Interplanetary Southward Magnetic Fields Responsible for Major Magnetic Storms Near Solar

580   Maximum (1978-1979), Journal of Geophysical Research, Vol. 93, No. A8, Pages 8519-8531,

581   Paper number 7A9404, 0148-0227/88/007 A-9404$05.00.

582 Tsurutani, B.T., Gonzalez, W.D., Lakhina, G.S. Alex, S., (2003). The extreme magnetic storm of

583   1-2 September 1859, J. Geophys. Res. 108(A7), doi: 10.1029/2002JA009504.

584   Tsurutani, B.T., Lakhina, G.S., Hajra, R., (2020), The physics of space weather/solar-terrestrial

585   physics (STP): what we know now and what the current and future challenges are, Nonlin.

586   Processes Geophys., 27, 75–119, doi:10.5194/npg-27-75-2020.

587   Tsurutani, B.T., Lakhina, G.S., Verkhoglyadova, O.P., Gonzalez, W.D., Echer, E., Guarnieri, F.L.,

588   (2010). A review of interplanertary discontinuities and their geomagnetic effects. Journal of

589   Atmospheric and Solar-Terrestrial Physics, doi: 10.1016/j.jastp.2010.04.001.

590   Tsutomu, N., (2002). Geomagnetic storms. Journal of communications Research Laboratory, Vol.

591   49, No.3.

592   Turner, N.E., Mitchell, E.J., Knipp, D.J., Emery, B.A., (2006), Energetics of magnetic storms

593   driven by corotating interaction regions: a study of geoeffectiveness, Geophysical Monograph

594   Series 167, 10.1029/167GM11.

595   Unikrishnan, K., (2008). Comparison of chaotic aspect of magnetosphere under various physical

596   conditions using AE index time series. Ann. Geophys., 26, 941-953, www.ann-

597   geophys.net/26/941/2008.

598   Unikrishnan, K., Ravindran, S., (2010). A study on chaotic behaviour of equatorial/low latitude

599   ionosphere over indian sub-continent, using GPS-TEC time series, J. Atmos. Sol. Ter. Phys.,

600   72, 1080-1089.

601   Valdivia, J.A., Rogan, J., Munoz, V., Gomberoff, L., Klimas, A., Vassilliasdis, D., Uritsky, V.,

602   Sharma, S., Toledo, B., Wastaviono, L. (2005). The magnetosphere as a complex system. Adv.

603   Space. Res, 35, 961-971.

604 Valdivia, J.A., Sharma, A.S., Papadopoulos, K., (1996). Prediction of magnetic storms by nonlinear

605   models. Geophysical Research Letters, 23(21), 2899-2902, doi: 10.1029/96GL02828.

606 Vassiliadis, D., (2006). Systems theory for geospace plasma dynamics, Rev.Geophys., 44, RG2002,

607   doi: 10.1029/2004RG000161.

608 Vassiliadis, D., Klimas, A.J., Valdivia, J.A., Baker, D.N., (1999). The geomagnetic response as a

609   function of storm phase and amplitude and solar wind electric field. Journal of Geophysical

610   Research, 104(A11), 24957-24976, doi: 10.1029/1999JA900185.

611 Vassilliadis, D., Sharma, A.S., Papadopoulos, K., (1991). Lyapunov exponent of magnetospheric

612   activity from AL time series. J. GeoPhys. Letts, Vol. 18, No.8, PP. 1643-1646.

613 Vassilliadis, D.V., Sharma, A.S., Eastman, T.E., Papadopoulou, K., (1990). Low-dimensional

614   chaos in magnetospheric activity from AE time series. J. GeoPhys.Res.Lett, 17, 1841-1844.

615 Wallot, S., Monster, D., (2018). Calculation of Average Mutual Information (AMI) and False

616   Nearest Neigbhours (FNN) for the estimation of embedding parameters of multidimensional

617   time series in MATLAB. Front. Physchol. 9:1679, doi: 10.3389/fpsyg.2018.01679.

618 Watari, S., (2017). Geomagnetic storms of cycle 24 and their solar sources, Earth, Planets and

619   Space, PP: 69:70, doi: 10.1186/s40623-017-0653-z.

620 Wolf, A., Swift, J. B., Swinney, H. L., and Vastano, J. A. (1985). Determining Lyapunov exponents

621   from a time series, *Physica D*, *16*, 285–317, doi:10.1016/0167-2789(85)90011-9.

622 Zhang, J., Dere, K.P., Howard, R.A., Bothmer, V., (2002), Identification of solar sources of major

623   geomagnetic storms between 1996 and 2000. Astrophysical Journal, 582:520-53.

624

625
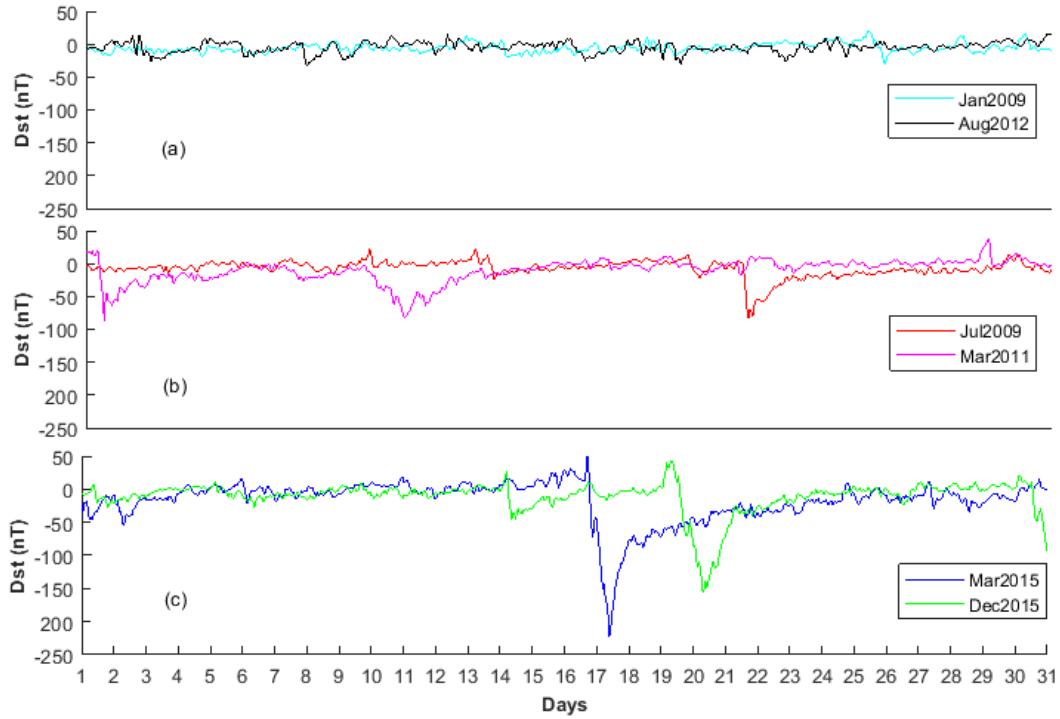
Figure 1: Samples of Dst signals classified as (a) Month of Minor, (b) Month of Moderate and (c)
Month of Major geomagnetic storm activity

628
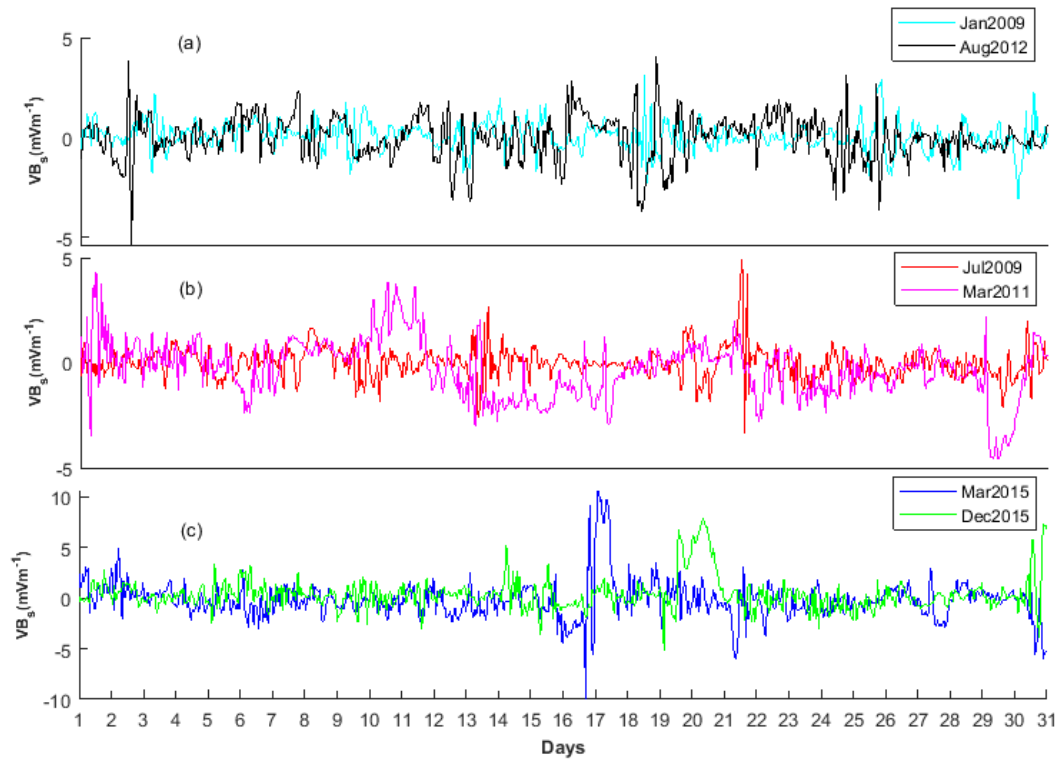
Figure 2: Samples of (VB_s) during (a) Month of Minor, (b) Month of Moderate and (c) Month of
Major geomagnetic storm activity.

631

632
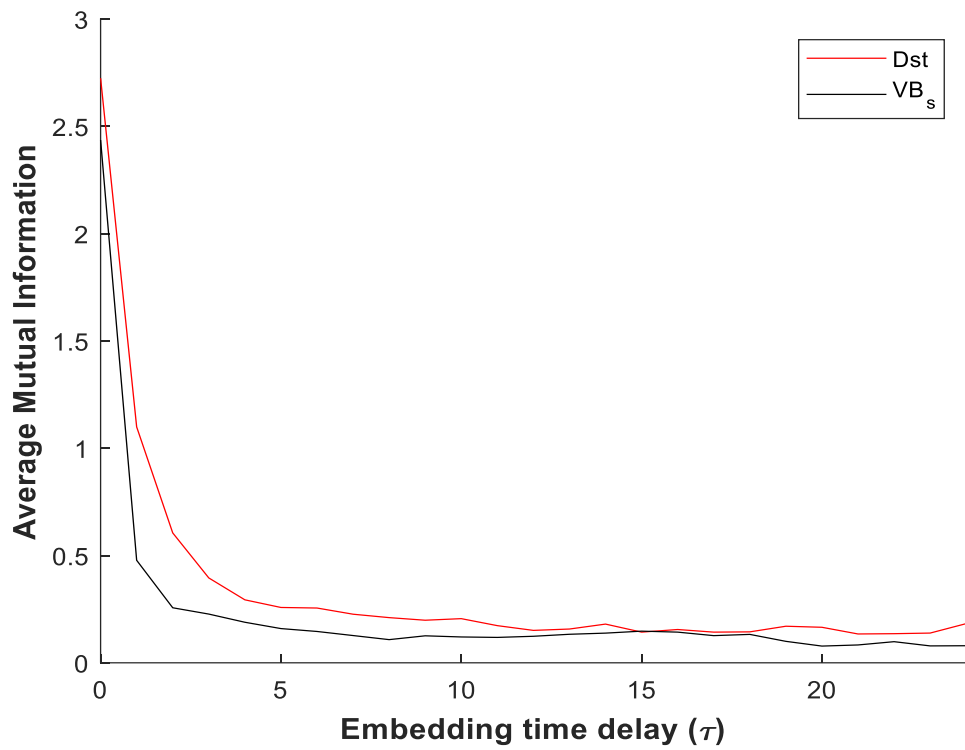
Figure 3: The plot AMI against embedding time delay (τ)

633

634
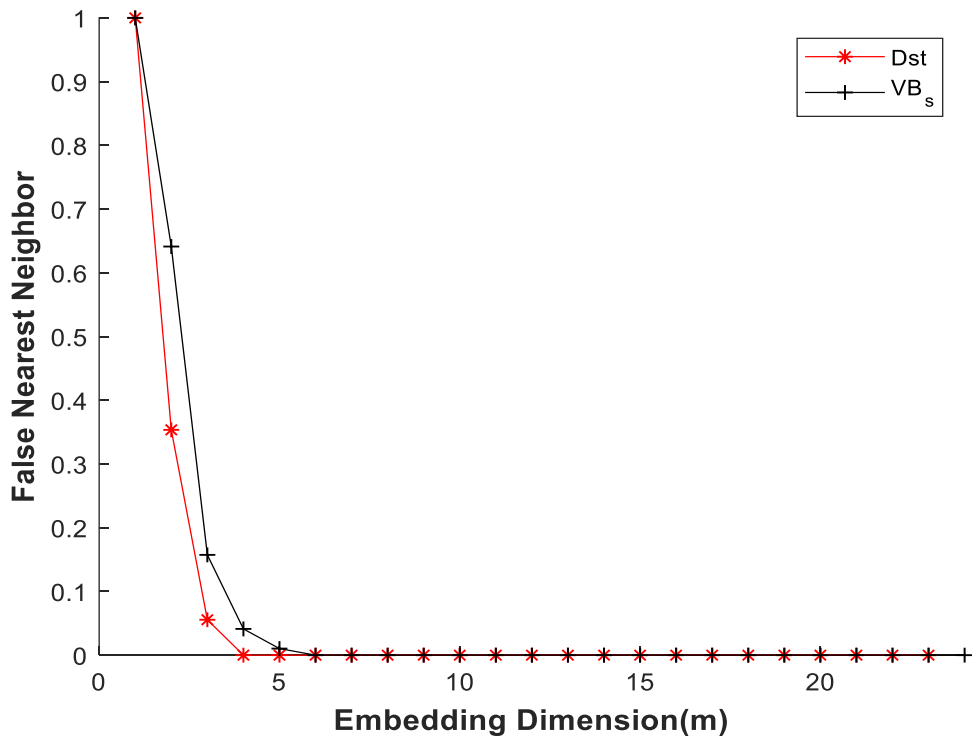
Figure 4: The plot of FNN against embedding dimension (m)

635
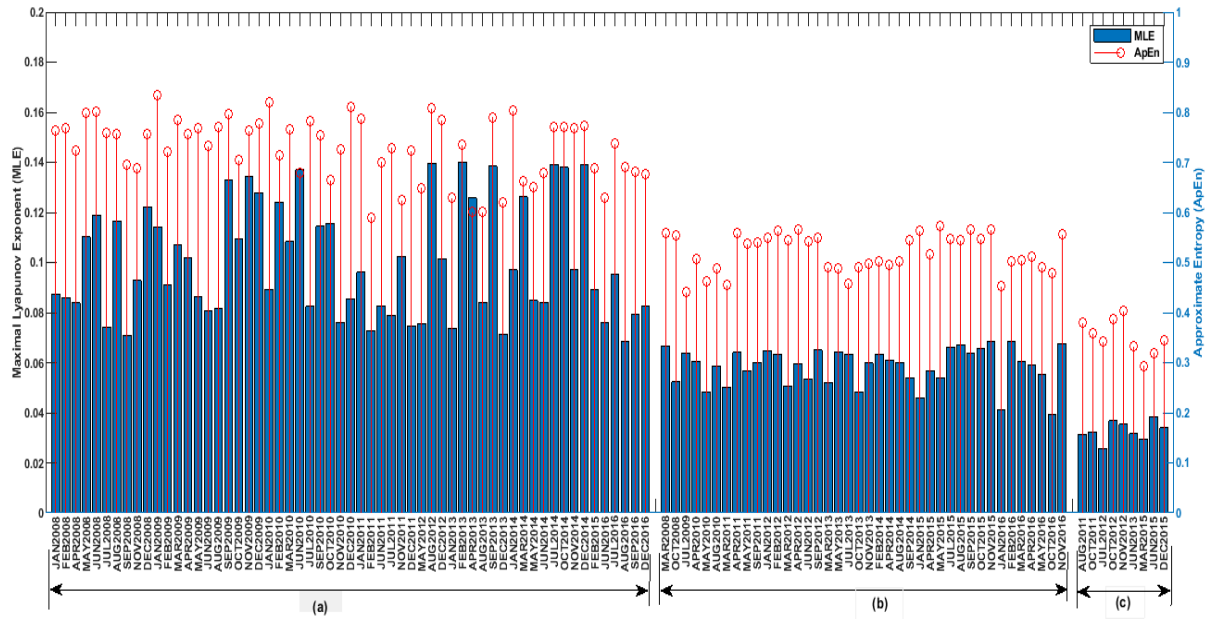
636

637 Figure 5: The MLE (bar plot) and ApEn (stem plot) of Dst at: (a) Month of Minor, (b) Month of
638 Moderate and (c) Month of Major geomagnetic storm activity

639

640

641

642

643

644

645
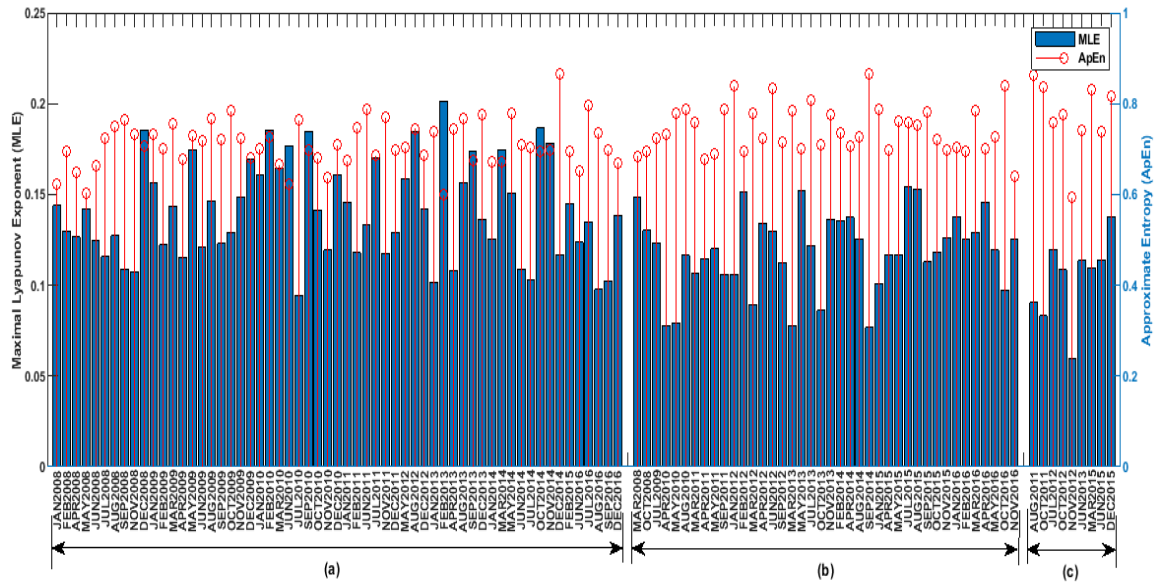
Figure 6: The MLE (bar plot) and ApEn (stem plot) of solar wind electric field (VB_s) during: (a) Month of Minor, (b) Month of Moderate and (c) Month of Major geomagnetic storm activity.

662
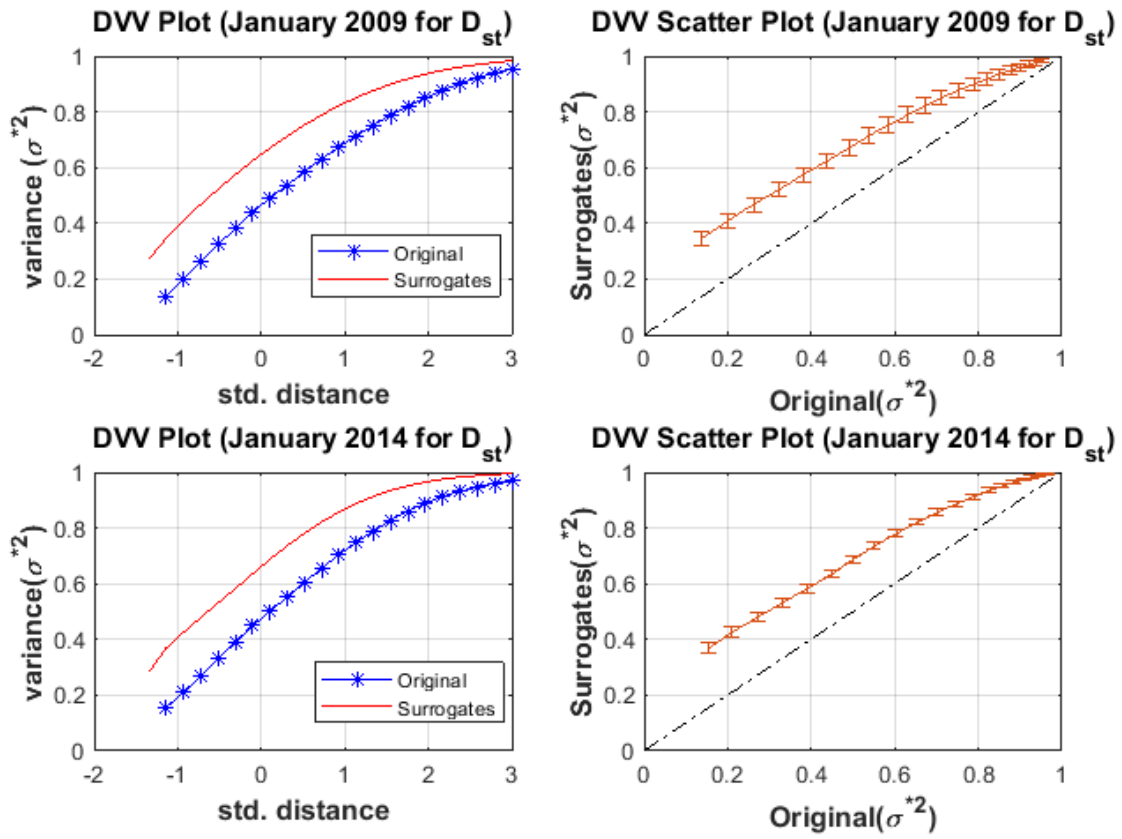
Figure 7: The DVV plot and Scatter plot for D_{st} during the month of minor geomagnetic storm
for January 2009 and January 2014.
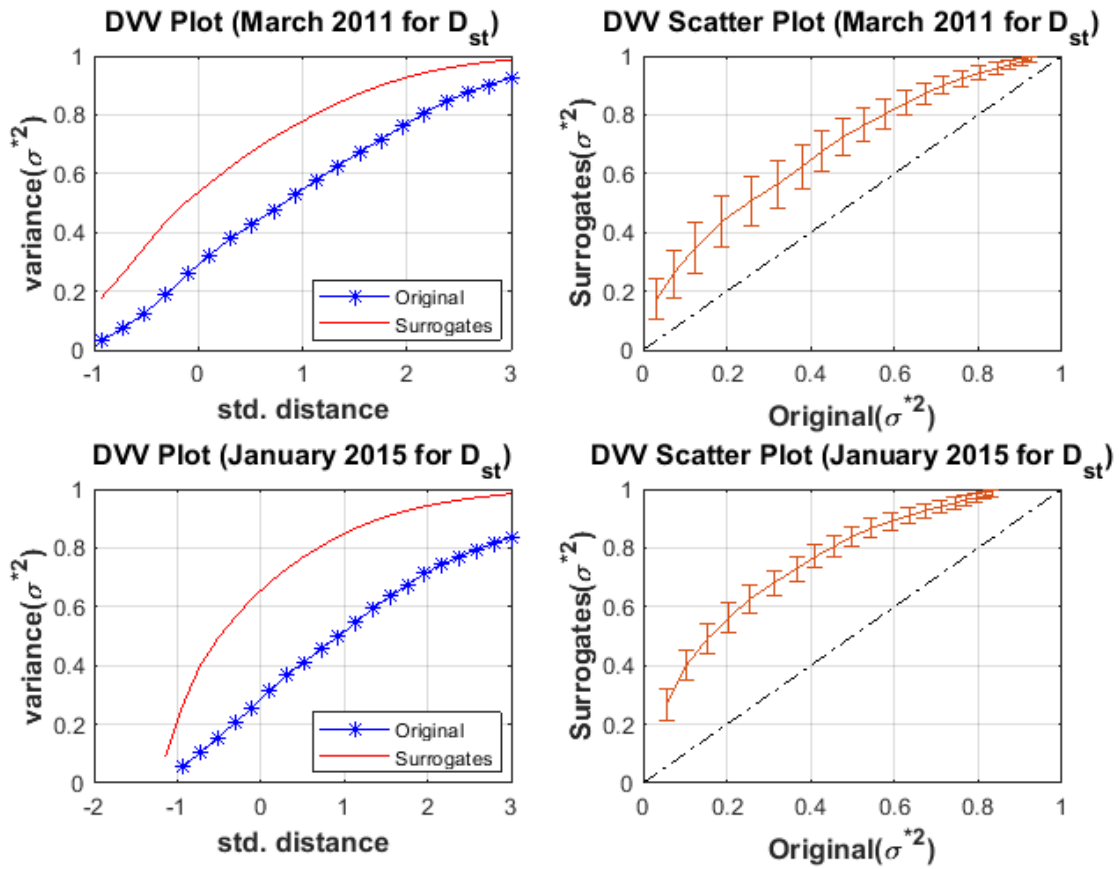
665

666

667 Figure 8: The DVV plot and Scatter plot for D_{st} during the month of moderate geomagnetic storm

668 for March 2011 and January 2015.

669
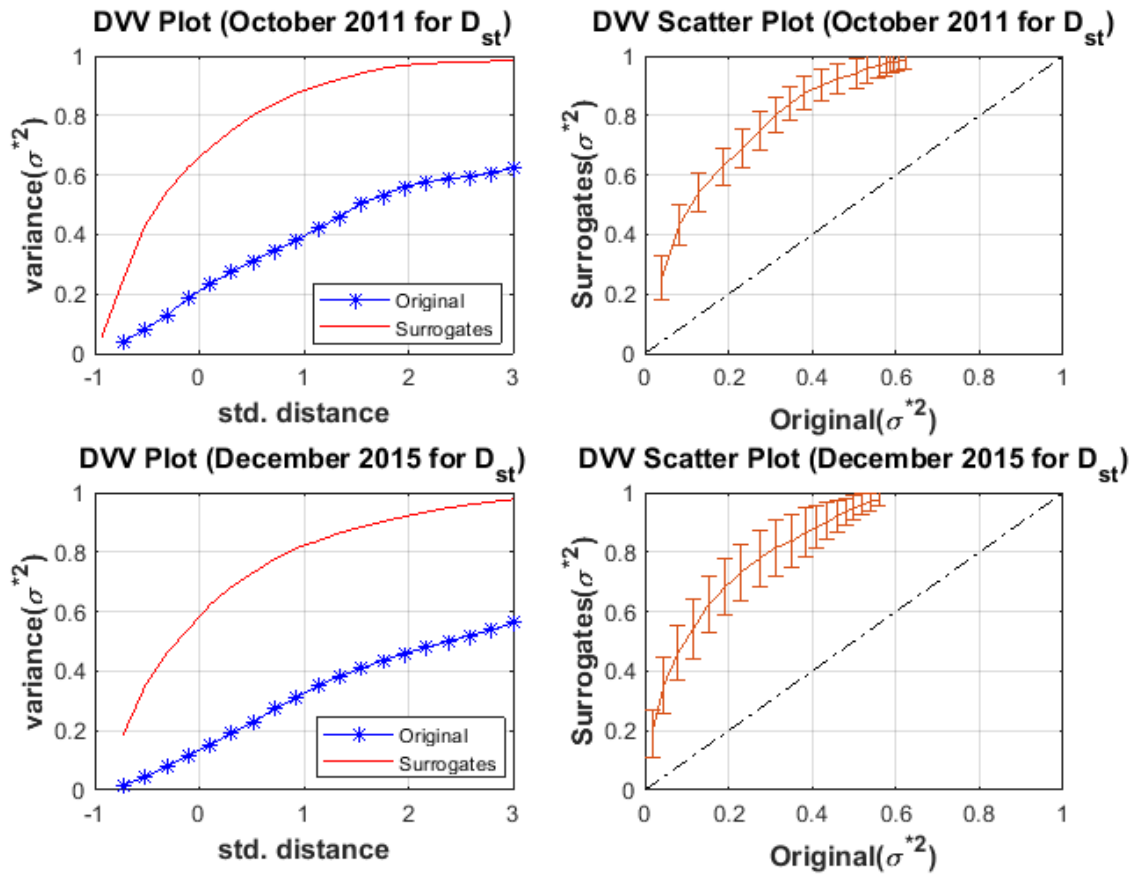
670

671   Figure 9: The DVV plot and Scatter plot for D_{st} during the month of major geomagnetic storm
672   for October 2011 and December 2015.

673
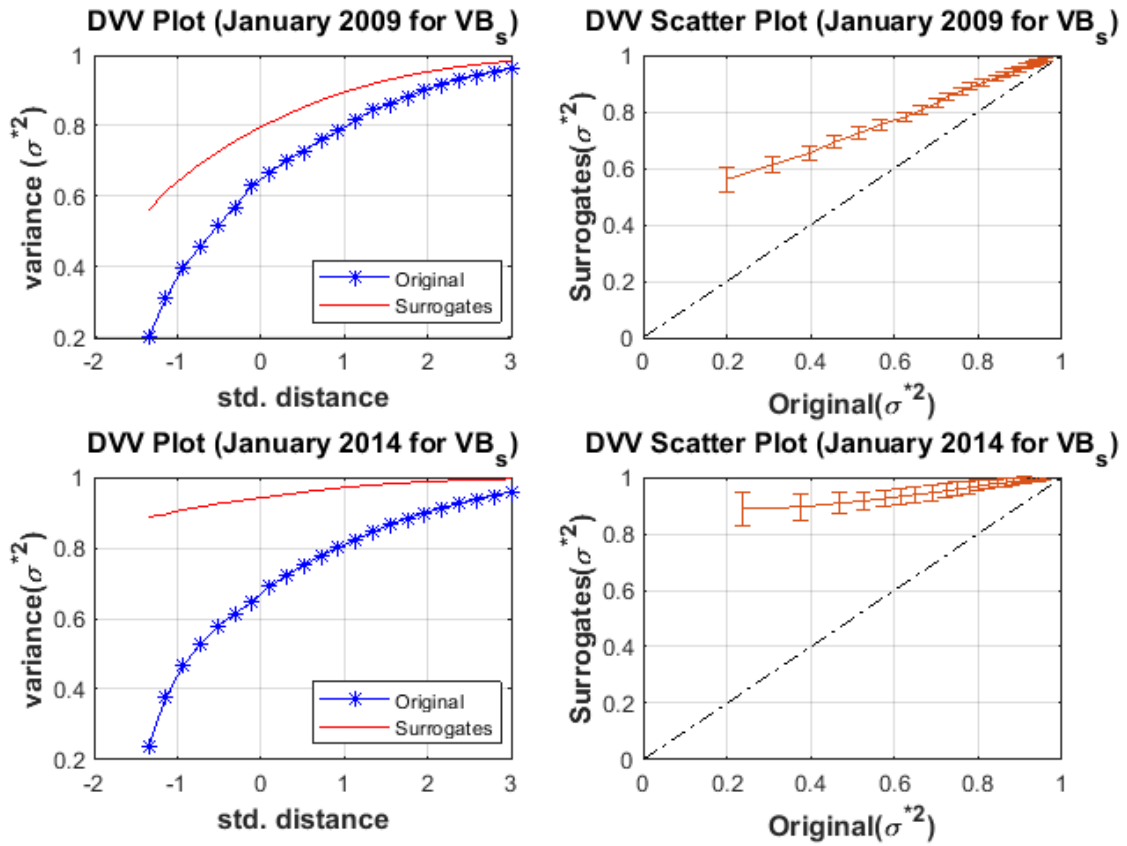
674

675 Figure 10: The DVV plot and Scatter plot for VB_s during the month of minor geomagnetic storm
676 for January 2009 and January 2014.

677

678
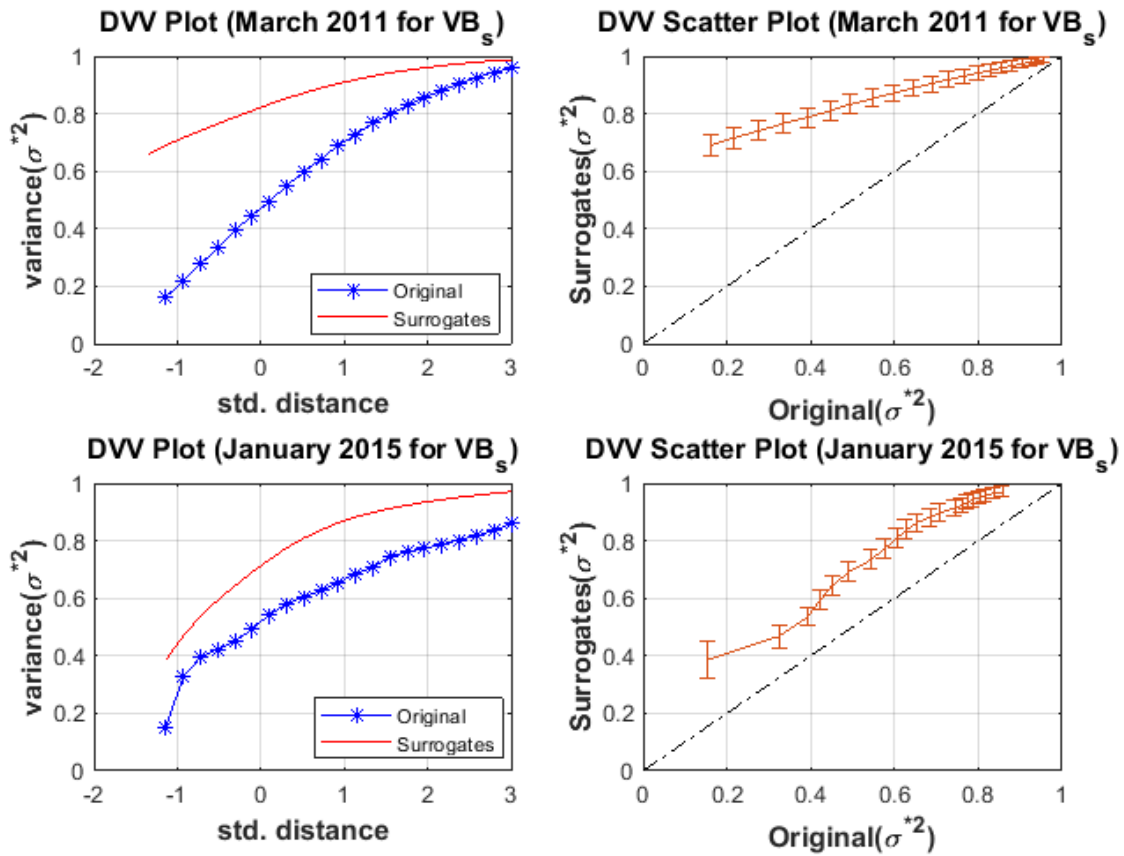
679

680   Figure 11: The DVV plot and Scatter plot for VB_s during the month of moderate geomagnetic
681   storm for March 2011 and January 2015.

682

683
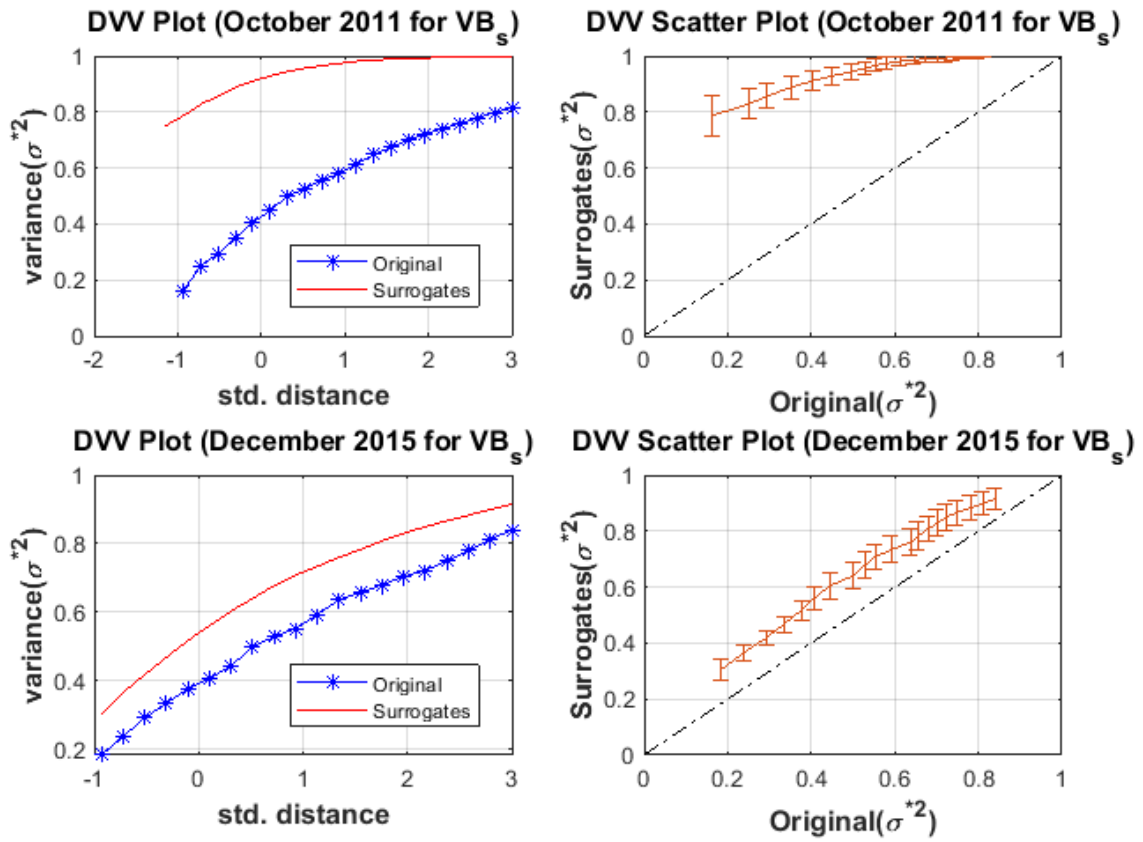
684

685 Figure 12: The DVV plot and Scatter plot for VB_s during the month of major geomagnetic storm

686 for October 2011 and December 2015.

687

688

689